



## Effective enhancement of electrochemical properties of LSM oxygen electrode in SOCs by LNO nano-catalyst infiltration

Zohreh Akbari, Alireza Babaei\*, Abolghasem Ataie

School of Metallurgy and Materials Engineering, College of Engineering, University of Tehran, Tehran, Iran.

Received: 30 October 2017; Accepted: 11 January 2018

\* Corresponding author email: [alireza.babaei@ut.ac.ir](mailto:alireza.babaei@ut.ac.ir)

### ABSTRACT

In this paper, the effects of infiltration of  $\text{La}_2\text{NiO}_4$  (LNO) as a mixed ionic and electronic conductor (MIEC) on the electrochemical performance of porous strontium doped lanthanum manganite (LSM) oxygen electrode of solid oxide cells, in the temperature ranges of 650-850 °C, is reported. XRD and FE-SEM results of the LNO sample calcined at 900 °C confirmed the formation of single phase LNO nanoparticles and uniform distribution of LNO into the porous LSM backbone with a mean particle size of 40 nm, respectively. To characterize the electrochemical behavior of half-cells, electrochemical impedance spectroscopy (EIS) measurement at temperature intervals of 50 °C was carried out. The LNO infiltrated LSM electrodes showed a noticeably decreased activation energy (from 130 to 103 kJ mol<sup>-1</sup>) and polarization resistance (from 26.2 to 2.5 Ωcm<sup>2</sup> at 650 °C) under open circuit voltage (OCV) condition. Besides, the equivalent circuit (EC) modeling revealed that LNO addition has a major effect on the low frequency arc, which is attributed to the surface exchange mechanisms. Decreased amounts of activation energy and polarization resistance of the infiltrated LSM electrode compared to those for the pure one suggest that introduction of LNO nano-particles to the microstructure of LSM is a promising approach to achieve better electrochemical performance even in the low temperature of 650°C.

**Keywords:**  $\text{La}_2\text{NiO}_4$ , solid oxide cell, LSM; Electro Catalyst, Infiltration.

### 1. Introduction

Solid oxide cells (SOCs) are high temperature (600-1000°C) electrochemical devices which can work in both fuel cells and electrolysis modes. In solid oxide fuel cells (SOFCs), chemical energy of a fuel (like hydrogen) is directly converted to electrical energy while solid oxide electrolysis cells (SOECs) works in reverse (1-3). Each solid oxide cell is mainly made from three parts: air electrode (oxygen electrode), fuel electrode and electrolyte (4-6). Chemical reactions take place in three- phase or two-phase boundaries (TPBs or 2PBs), which electrode, electrolyte and gas reactant

are present. One of the technical barriers to the development of the SOCs is the matter of materials used in electrodes, especially in air electrode (6, 7). Strontium doped lanthanum manganite (LSM) is one of the most studied materials for the oxygen electrode in solid oxide cells (SOCs) (7-9). LSM is a very good thermally activated electron conductor and has an excellent electro-catalytic activity for the  $\text{O}_2$  reduction/oxidation reaction at high temperatures. For this reason, it has been used widely in this context. However, the conductivity of LSM is limited to electron conduction and practically has no ionic conduction even at high

temperatures (4, 7-9). Based on Jiang's reports, polarization resistance ( $R_p$ ) of LSM is as high as  $8 \Omega \cdot \text{cm}^2$  at  $800^\circ\text{C}$  for oxygen reduction reaction (10-12). In such electron conductor electrodes, TPBs play a major role in the cell performance, therefore the quality and quantity of these TPBs are of great importance (1, 13). To get high performance from a solid oxide cell with LSM oxygen electrode, different approaches are proposed to extend reaction sites into the bulk of electrode (13-16). One of them is introducing a nanostructured ionic conductor or mixed ionic and electronic conductor (MIEC) phase into LSM backbone by infiltration technique (17, 18). By this approach, enhancement of durability, structural stability and electro-catalytic activity of electrode is expected. Jiang showed that infiltration of gadolinium doped ceria (GDC) into LSM electrode has improved the polarization response of the cell (10). It has also been reported that electro-catalytic activity of LSM was significantly improved and  $R_p$  was reached to a smaller value of 3.19 and  $0.89 \Omega \cdot \text{cm}^2$  at  $700^\circ\text{C}$  by infiltration of NdN ( $\text{Nd}_{1.95}\text{NiO}_{4+\delta}$ ) and SDC ( $\text{Sm}_{0.5}\text{Sr}_{0.5}\text{CoO}_{3-\delta}$ ), respectively (19).

One requirement of electrodes is chemical stability in both oxidation and reduction environments. Nickelates with Ruddlesden–Popper structure such as  $\text{La}_2\text{NiO}_4$  (LNO) are MIECs materials which are satisfying this requirement (20-22). It has been shown that infiltration of LNO into LSCF oxygen electrode has enhanced performance and stability of the electrode (23-25). In another study, infiltration of LNO on the GDC backbone was investigated and the results showed that infiltration of a MIEC material into an ionic conductor is a very promising route to significantly increase the electrochemical performance of the cell (25).

Therefore, infiltration of nickelates into LSM backbone seems to be a promising method to improve cell performance and reduce degradation by increasing TPBs and extending reaction sites into the electrode bulk.

In the present study, the activation energy and electrochemical performance of the non-infiltrated LSM and LNO infiltrated LSM oxygen electrodes were systematically studied under open circuit voltage (OCV).

## 2. Experimental

Electrolyte pellets were prepared by die pressing of YSZ powder (8 mol%  $\text{Y}_2\text{O}_3$  stabilized  $\text{ZrO}_2$ ,

Tosoh, Japan) at 70 Mpa followed by sintering at  $1500^\circ\text{C}$  for 6h. Thickness and diameter of sintered pellets were 1 and 19 mm, respectively. Asymmetric cell configuration with three electrodes was selected for the electrochemical measurements. In one side of electrolytes, LSM (Fuel Cell Materials, USA) ink was painted as the working electrode with the area of  $0.385 \text{ cm}^2$  and on the other side of pellets Pt ink (6082 Metalor, Swiss) was applied as the counter electrodes, opposite to the working electrode. Reference electrode was painted as a ring around counter electrode on the back side circumference of YSZ pellets. Pt ink was fired at  $850^\circ\text{C}$  for 15 min and LSM ink was sintered at  $1100^\circ\text{C}$  for 2h.

To realize the formation of LNO phase, LNO powder was synthesized in a separate beaker by citrate–nitrate combustion technique. Lanthanum nitrate ( $\text{La}(\text{NO}_3)_3 \cdot 6\text{H}_2\text{O}$ ) and nickel nitrate ( $\text{Ni}(\text{NO}_3)_2 \cdot 6\text{H}_2\text{O}$ ) with a molar ratio of La:Ni equal to 2:1 were dissolved in 10 mL of deionized water. Then, citric acid (CA) was mixed into the solution as the ligand with the molar ratio of La:Ni:CA = 2:1:3. The complex solution was heated to  $60^\circ\text{C}$  until a gel was formed and then dried at  $100^\circ\text{C}$  for 20h, followed by combustion at  $350^\circ\text{C}$  and calcination at  $900^\circ\text{C}$  for 2h. The phase composition was characterized by X-ray diffraction (XRD) (Philips, PW 1730) at room temperature using  $\text{Cu-K}_\alpha$  radiation ( $\lambda=1.5406 \text{ \AA}$ ).

Multiple infiltration steps were carried out by impregnating a single drop of 0.5M complex solution into the porous LSM electrode with Pasteur pipettes for four times. The infiltrated cells were subsequently fired at  $900^\circ\text{C}$  for 2 h to form the LNO phase over the LSM backbone.

To investigate the electrochemical response and activation energy of the infiltrated and non-infiltrated cells, electrochemical impedance spectroscopy (EIS) was carried out under open circuit voltage (OCV) at the temperature range of  $650\text{-}800^\circ\text{C}$  using a PARSRAT 2273 potentiostat. Impedance spectra were obtained in the frequency range of 10 mHz to 100 kHz with signal amplitude of 10 mV.

Finally, the microstructure of the infiltrated and non-infiltrated cells was investigated by field emission scanning electron microscope (TESCAN).

## 3. Results & Discussion

Fig. 1a displays the XRD pattern of LNO powder calcinated at  $900^\circ\text{C}$  for 2h. Analysis of the XRD pattern confirms the formation of Ruddlesden–

Popper single phase ( $\text{La}_2\text{NiO}_4$ ) with a tetragonal crystal structure (with the reference card No. 01-080-1910). The XRD pattern in Fig. 1a is compared with the reference data shown in Fig. 1b. However, since the synthesis was under oxidative condition, oxygen non-stoichiometry ( $\text{La}_2\text{NiO}_{4+\delta}$ ) is expected (26, 27). FE-SEM micrograph of the cross-section of the prepared half cell, as well as the micrographs of the non-infiltrated and LNO infiltrated LSM electrodes are depicted in Fig. 2. The thickness of the electrode layer is measured around  $30\ \mu\text{m}$  in Fig. 2a. The microstructure of the LSM electrode is characterized by the well interconnected smooth LSM particles with approximate size of  $0.5\text{-}1\ \mu\text{m}$

(Fig. 2b). In the case of the infiltrated electrode (Fig. 2c), LNO nanoparticles with a mean particle size of  $40\ \text{nm}$  are observed. LNO nanoparticles are also well distributed on the surface of LSM electrode particles. This would promote the formation of more TPBs for oxygen reduction reactions.

Fig. 3 exhibits the electrochemical impedance spectroscopy (EIS) curves for non-infiltrated and LNO infiltrated LSM electrodes at open circuit voltage (OCV) in the temperature range of  $650\text{-}850\ ^\circ\text{C}$  with the interval of  $50\ ^\circ\text{C}$ . In the impedance curves, polarization resistances ( $R_p$ ) were obtained from the differences between the high and low frequency intercepts on the real axis and the ohmic

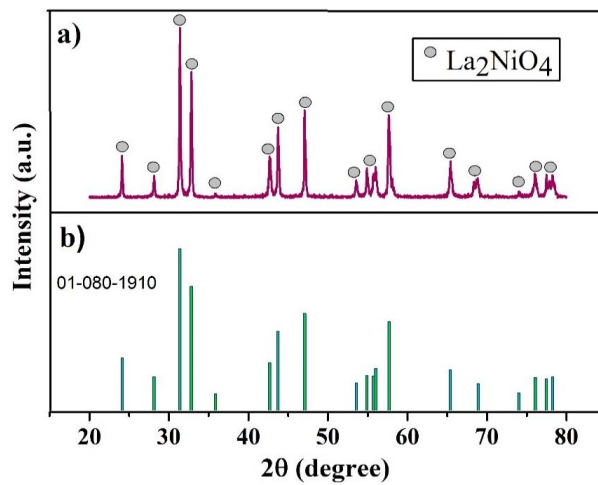


Fig. 1- XRD pattern of a) LNO powder calcined at  $900\ ^\circ\text{C}$  for 2h and b) the reference card of  $\text{La}_2\text{NiO}_4$  phase (01-080-1910).

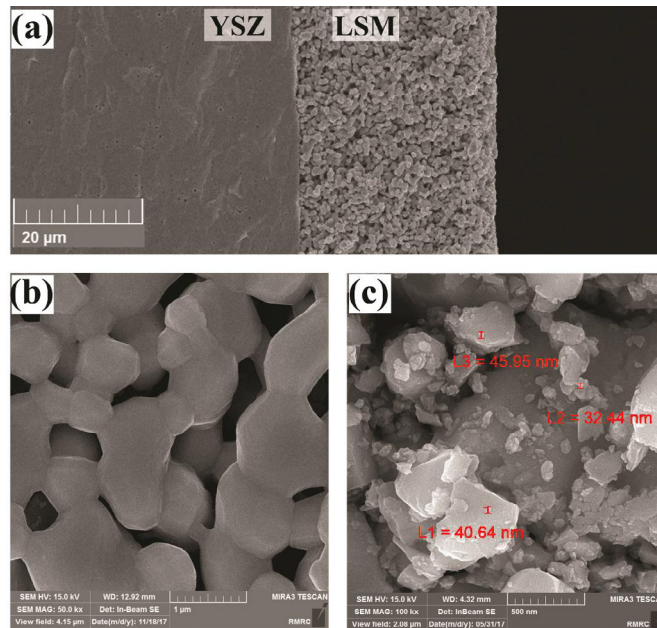


Fig. 2- FESEM micrographs of a) cross-section of prepared cell, b) non-infiltrated and c) LNO infiltrated LSM electrodes.

resistance was obtained from high frequency intercept of the impedance spectra.

In both LNO infiltrated and non-infiltrated LSM electrodes,  $R_p$  and  $R_\Omega$  follow a decreasing trend with increasing temperature. Reduction in  $R_p$  (for example: from 26.21 to 2.52  $\Omega\cdot\text{cm}^2$  at 650 °C and from 2.95 to 0.37  $\Omega\cdot\text{cm}^2$  at 800 °C) and  $R_\Omega$  are caused by thermally activated electronic conduction in LSM and thermally activated ionic conduction in YSZ, respectively. However, addition of LNO nanoparticles, has a great impact on the reduction of polarization resistance of oxygen reduction/oxidation reactions. This reduction is occurred due to the several causes including; (1) provision of more active surface for oxygen reduction/oxidation

reactions by adding MIEC nano-sized particles (i.e. introducing two phase boundaries to the system), (2) increasing TPBs as a result of nanoparticle insertion, (2) high intrinsic diffusion rate of oxygen ion and surface exchange coefficient of LNO which accelerate the kinetic of oxygen reduction/oxidation reactions.

Detailed study of the impedance spectra of the non-infiltrated and LNO infiltrated LSM electrodes by means of equivalent circuit (EC) modeling revealed biased influence of LNO infiltration on different steps of the oxygen reduction/oxidation reaction. In the case of non-infiltrated LSM electrode (Fig. 4), there are two main arcs at high and low frequency portions of impedance spectra

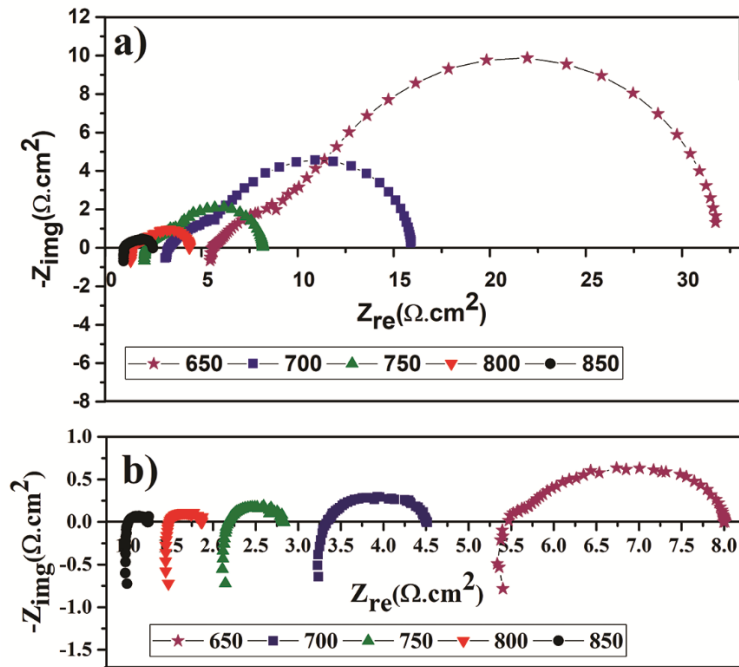


Fig. 3- EIS spectra for a) non-infiltrated and b) LNO infiltrated LSM electrodes in temperature range of 650-850°C.

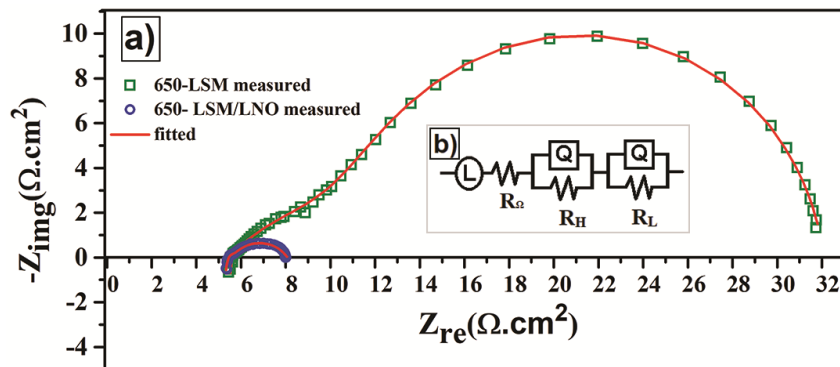


Fig. 4- a) Measured and fitted impedance spectra of LNO infiltrated and non-infiltrated LSM electrode and b) EC modeling of LNO infiltrated and non-infiltrated LSM electrode.

which are associated with oxygen reduction/oxidation reaction on the TPBs (18). Low frequency arc is related to the oxygen dissociation (or association) and/or surface diffusion processes of oxygen species (1, 28, 29). In the literatures, different interpretations for the high frequency arc were declared. Jiang et al. reported that the high frequency arc is attributed to oxygen ion migration from the LSM electrode to the YSZ electrolyte (or vice versa) (28, 30, 31) while Heuveln is considered that as a subsequent result of charge transferring mechanism (32, 33).  $R_{\Omega}$  is ohmic resistance and apart from the resistance of the wires, it also displays the resistance between the LSM electrode and Pt counter electrode, which includes interface resistance (between electrodes and electrolyte) and electrolyte resistance (1, 10, 28-33).

An inductance tail at high frequencies is observed in all EIS curves which is originated mainly from connecting wires and setup system. This inductance effect is depicted with an inductance (L) in EC model. Fig. 4b shows the EC modeling of the LSM-based electrode which consists of two RQ series with one  $R_{\Omega}$  and L, in which R represents resistance

and Q is phase constant element. The subscript L and H denotes low frequency and high frequency elements, respectively. EIS curves that modeled with this EC by means of Zsimpwin software, are shown in Fig. 4a. It can be seen that the fitted data is in good agreement with measured ones. The extracted data from fitted curves ( $R_L$  and  $R_H$ ), are graphed in Fig. 5.

Both high and low frequency arcs are affected by temperature; however, the change in  $R_L$  is more impressive. As temperature rises,  $R_L$ s become smaller, more considerably compared to  $R_H$ s. This shows that oxygen dissociation (or association) and/or surface diffusion processes have been improved more significantly compared to charge transfer and/or oxygen ion migration process, by infiltration of a MIEC.

Polarization resistance of the electrodes was extracted from EIS curves and sketched as a function of reverse temperature ( $T^{-1}$ ) in logarithmic coordinate (Fig. 6). According to the Eq. (1),  $R_p$  has an Arrhenius-type dependency to  $T^{-1}$  [28].

$$R_p = A \exp\left(\frac{-E_a}{RT}\right) \quad (\text{eq. 1})$$

where, A is an empirical pre-exponential constant, R is the universal gas constant equal to  $8.314 \text{ J}\cdot\text{mol}^{-1}\cdot\text{K}^{-1}$ . From this formula, activation energy for the oxygen reduction/oxidation reaction is calculated equal to  $130.38 \text{ kJ}\cdot\text{mol}^{-1}$  for non-infiltrated LSM and  $103.16 \text{ kJ}\cdot\text{mol}^{-1}$  for 2M LNO infiltrated LSM cell.  $E_a$  value for non-infiltrated LSM is in accordance with previous studies (34-37). In general terms, by incorporation of a catalyst the activation energy for the desired reaction decreases, as a lower

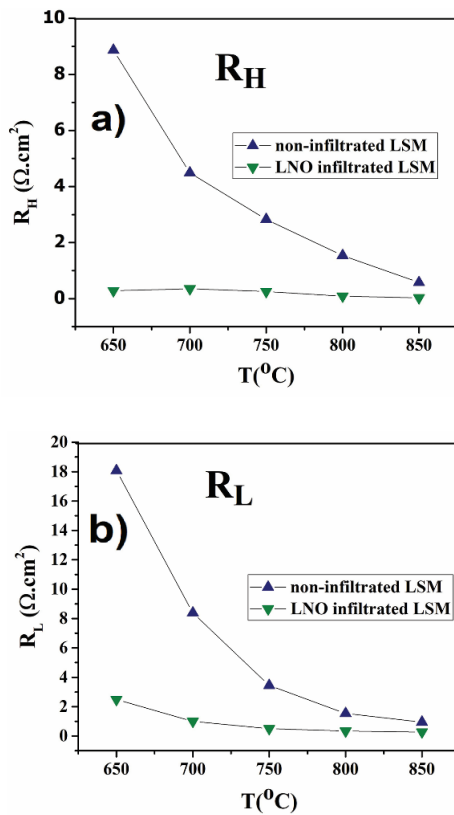


Fig. 5- Effect of temperature and LNO impregnation on a) RH and b) RL of EIS curves of LSM backbone

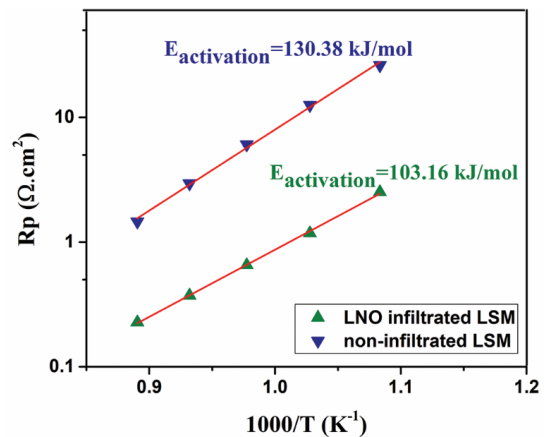


Fig. 6- Arrhenius plots of  $R_p$  vs  $1000/T$ , for the oxygen reduction reaction on the non-infiltrated and LNO infiltrated LSM electrode.

energy transition state is formed. Since LNO is a MIEC, its infiltration into the LSM backbone as an electro-catalyst may provide alternate reaction pathways with lower activation energies causing a drop of 21% in the activation energy of the oxygen reduction reaction.

#### 4. Conclusions

In this study, activation energy for the oxygen reduction/oxidation reaction as well as electrochemical behavior of non-infiltrated and LNO infiltrated LSM oxygen electrode was investigated at different temperatures under OCV condition. Results show that presence of LNO nanoparticles on the LSM surface, effectively expands the reaction sites from TPBs to the LSM electrode/LNO nanoparticle interface in the electrode bulk. Thus, substantially enhanced the activity of the LSM-based oxygen electrodes. Therefore, infiltration of LNO into LSM backbone is a promising approach to achieve better electrochemical performance even in the intermediate temperature range of 600-800 °C.

#### Acknowledgment

The authors would like to acknowledge University of Tehran (grant No. 810729920/6/02) and Iran Nanotechnology Initiative Council (grant No. 121046) for their financial supports.

#### References

- Jiang SP. Development of lanthanum strontium manganite perovskite cathode materials of solid oxide fuel cells: a review. *Journal of Materials Science*. 2008;43(21):6799-833.
- Jiang SP. Challenges in the development of reversible solid oxide cell technologies: a mini review. *Asia-Pacific Journal of Chemical Engineering*. 2016;11(3):386-91.
- Rayment C, Sherwin S. Introduction to fuel cell technology. Department of Aerospace and Mechanical Engineering, University of Notre Dame, Notre Dame, IN. 2003 May 2;46556:11-2.
- Perovskite Oxide for Solid Oxide Fuel Cells. *Fuel Cells and Hydrogen Energy*; Springer US; 2009.
- Ni M, Leung M, Leung D. Technological development of hydrogen production by solid oxide electrolyzer cell (SOEC). *International Journal of Hydrogen Energy*. 2008;33(9):2337-54.
- Brisse A, Schefold J, Zahid M. High temperature water electrolysis in solid oxide cells. *International Journal of Hydrogen Energy*. 2008;33(20):5375-82.
- Electrochemical Energy*; CRC Press; 2015 2015/12/10.
- Borowski M. Perovskites: structure, properties, and uses. Nova Science Publishers; 2010.
- Babaei A, Zhang L, Liu E, Jiang SP. Performance and stability of La<sub>0.8</sub>Sr<sub>0.2</sub>MnO<sub>3</sub> cathode promoted with palladium based catalysts in solid oxide fuel cells. *Journal of Alloys and Compounds*. 2011;509(14):4781-7.
- Chen K, Ai N, Jiang SP. Performance and structural stability of Gd<sub>0.2</sub>Ce<sub>0.8</sub>O<sub>1.9</sub> infiltrated La<sub>0.8</sub>Sr<sub>0.2</sub>MnO<sub>3</sub> nano-structured oxygen electrodes of solid oxide electrolysis cells. *International Journal of Hydrogen Energy*. 2014;39(20):10349-58.
- Chen K, Ai N, Jiang SP. Enhanced electrochemical performance and stability of (La,Sr)MnO<sub>3</sub>-(Gd,Ce)O<sub>2</sub> oxygen electrodes of solid oxide electrolysis cells by palladium infiltration. *International Journal of Hydrogen Energy*. 2012;37(2):1301-10.
- Wang W, Jiang S. A mechanistic study on the activation process of (La, Sr)MnO<sub>3</sub> electrodes of solid oxide fuel cells. *Solid State Ionics*. 2006;177(15-16):1361-9.
- Irvine JTS, Neagu D, Verbraeken MC, Chatzichristodoulou C, Graves C, Mogensen MB. Evolution of the electrochemical interface in high-temperature fuel cells and electrolyzers. *Nature Energy*. 2016;1(1):15014.
- Carpanese MP, Clematis D, Bertei A, Giuliano A, Sanson A, Mercadelli E, et al. Understanding the electrochemical behaviour of LSM-based SOFC cathodes. Part I — Experimental and electrochemical. *Solid State Ionics*. 2017;301:106-15.
- Bertei A, Carpanese MP, Clematis D, Barbucci A, Bazant MZ, Nicoletta C. Understanding the electrochemical behaviour of LSM-based SOFC cathodes. Part II - Mechanistic modelling and physically-based interpretation. *Solid State Ionics*. 2017;303:181-90.
- Vohs JM, Gorte RJ. High-Performance SOFC Cathodes Prepared by Infiltration. *Advanced Materials*. 2009;21(9):943-56.
- Ding D, Li X, Lai SY, Gerdes K, Liu M. Enhancing SOFC cathode performance by surface modification through infiltration. *Energy & Environmental Science*. 2014;7(2):552.
- Seyed-Vakili SV, Babaei A, Ataie M, Heshmati-Manesh S, Abdizadeh H. Enhanced performance of La 0.8 Sr 0.2 MnO 3 cathode for solid oxide fuel cells by co-infiltration of metal and ceramic precursors. *Journal of Alloys and Compounds*. 2018;737:433-41.
- Dailly J, Delrue A, Ancelin M, Marrony M. Nanoparticles Infiltration into SOFC Cathode Backbones. *ECS Transactions*. 2017;78(1):1979-91.
- Egger A, Schrödl N, Gspan C, Sitte W. La<sub>2</sub>NiO<sub>4+δ</sub> as electrode material for solid oxide fuel cells and electrolyzer cells. *Solid State Ionics*. 2017;299:18-25.
- Mauvy F, Lalanne C, Bassat JM, Grenier JC, Zhao H, Dordor P, et al. Oxygen reduction on porous Ln<sub>2</sub>NiO<sub>4+δ</sub> electrodes. *Journal of the European Ceramic Society*. 2005;25(12):2669-72.
- Cetin D. Thermodynamic stability of perovskite and lanthanum nickelate-type cathode materials for solid oxide fuel cells (Doctoral dissertation).
- Zhang X, Zhang H, Liu X. High performance La<sub>2</sub>NiO<sub>4+δ</sub> infiltrated (La 0.6 Sr 0.4 ) 0.995 Co 0.2 Fe 0.8 O 3-δ cathode for solid oxide fuel cells. *Journal of Power Sources*. 2014;269:412-7.
- Zhang X, Li W, Guan B, Liu X. A-Site Deficient La<sub>2</sub>XNiO<sub>4+δ</sub>Infiltrated LSCF Cathode with Improved Performance and Stability. *ECS Transactions*. 2017;78(1):593-601.
- Nicollet C, Flura A, Vibhu V, Rougier A, Bassat JM, Grenier JC. La<sub>2</sub>NiO<sub>4+δ</sub> infiltrated into gadolinium doped ceria as novel solid oxide fuel cell cathodes: Electrochemical performance and impedance modelling. *Journal of Power Sources*. 2015;294:473-82.
- Dong X, Wu Z, Chang X, Jin W, Xu N. One-Step Synthesis and Characterization of La<sub>2</sub>NiO<sub>4+δ</sub>Mixed-Conductive Oxide for Oxygen Permeation. *Industrial & Engineering Chemistry Research*. 2007;46(21):6910-5.
- Paulus W, Cousson A, Dhalenne G, Berthon J, Revcolevschi A, Hosoya S, et al. Neutron diffraction studies of stoichiometric and oxygen intercalated La<sub>2</sub>NiO<sub>4</sub> single crystals. *Solid State Sciences*. 2002;4(5):565-73.
- Li N, Ai N, Chen K, Cheng Y, He S, Saunders M, et al. In situ assembled La<sub>0.8</sub>Sr<sub>0.2</sub>MnO<sub>3</sub> cathodes on a Y<sub>2</sub>O<sub>3</sub>-ZrO<sub>2</sub> electrolyte of solid oxide fuel cells – interface and electrochemical activity. *RSC Advances*. 2016;6(101):99211-9.
- Perry Murray E. (La,Sr)MnO<sub>3</sub>-(Ce,Gd)O<sub>2-x</sub> composite cathodes for solid oxide fuel cells. *Solid State Ionics*. 2001;143(3-4):265-73.
- Chen X. Electrochemical behavior of La(Sr)MnO<sub>3</sub> electrode under cathodic and anodic polarization. *Solid State Ionics*. 2004;167(3-4):379-87.

31. Jiang SP, Zhang JP, Foger K. Deposition of Chromium Species at Sr-Doped  $\text{LaMnO}_3$  Electrodes in Solid Oxide Fuel Cells II. Effect on  $\text{O}_2$  Reduction Reaction. *Journal of The Electrochemical Society*. 2000;147(9):3195.
32. van Heuveln FH. Electrode Properties of Sr-Doped  $\text{LaMnO}_3$  on Yttria-Stabilized Zirconia. *Journal of The Electrochemical Society*. 1997;144(1):134.
33. van Heuveln FH. Electrode Properties of Sr-Doped  $\text{LaMnO}_3$  on Yttria-Stabilized Zirconia. *Journal of The Electrochemical Society*. 1997;144(1):126.
34. Jiang Z, Zhang L, Feng K, Xia C. Nanoscale bismuth oxide impregnated (La,Sr) $\text{MnO}_3$  cathodes for intermediate-temperature solid oxide fuel cells. *Journal of Power Sources*. 2008;185(1):40-8.
35. Jiang Z, Zhang L, Cai L, Xia C. Bismuth oxide-coated (La,Sr)  $\text{MnO}_3$  cathodes for intermediate temperature solid oxide fuel cells with yttria-stabilized zirconia electrolytes. *Electrochimica Acta*. 2009;54(11):3059-65.
36. Zhang QS, Hirano A, Imanishi N, Takeda Y, Yamahara K. LSM Cathodes Infiltrated With  $\text{Er}_2\text{O}_3$  Stabilized  $\text{Bi}_2\text{O}_3$ . *Journal of Fuel Cell Science and Technology*. 2009;6(1):011001.
37. Ai N, Jiang SP, Lü Z, Chen K, Su W. Nanostructured (Ba,Sr)(Co,Fe) $\text{O}_{3-\delta}$  Impregnated (La,Sr) $\text{MnO}_3$  Cathode for Intermediate-Temperature Solid Oxide Fuel Cells. *Journal of The Electrochemical Society*. 2010;157(7):B1033.